A High-Precision Extensometer System for Ground Displacement Measurement using Fiber Bragg Grating

M. A. Alias, M. F. Ismail, M. S. M. Sa'ad, M. K. A. Zaini, K. S. Lim, *Senior Member*, *IEEE*, K. T. V. Grattan, G. Brambilla, *Member*, *IEEE*, B. M. A. Rahman, *Life Fellow*, *IEEE*, S. A. Reduan and H. Ahmad

***Abstract*— The design and performance of an innovative high-precision extensometer system, fabricated inexpensively using 3D printing technology, are discussed in this paper. In the development of the extensometer, an embedded Fiber Bragg Grating (FBG) strain sensor was 3D printed using a thermoplastic polyurethane (TPU) filament, which was used as the primary sensing element of the extensometer system, taking advantage of its excellent flexibility and high sensitivity to variations in localized strain. In the performance assessment carried out, the results obtained during the experimental test and validation have demonstrated that it could be used very effectively to measure strain variations, with an average wavelength responsivity of 0.0158 nm/cm (for displacement) and very high linearity (up to 99%). Furthermore, the protection integrated into the sensor systems design makes it well-suited for in-the-field applications, such as monitoring ground displacements which can lead to dangerous slippages of sloped earthworks. In addition, a field testing of the extensometer under simulated conditions has shown that a Fiber Bragg Grating (FBG)-based approach could be applied effectively to the measurement of strain, offering a wavelength responsivity of 0.0012 nm/με (for strain-sensitive FBGs) under both dry and wet soil conditions. Moreover, taking advantage of the high (~99%) linearity, the extensometer is a reliable instrument for use in different underground conditions, creating an easy-to-use ground movement monitoring system which then enables an excellent representation of the displacement profile of the earth to be made.**

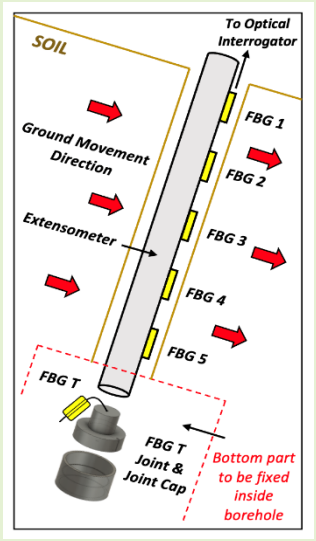

***Index Terms*—Extensometer, strain measurements, fiber Bragg grating-based technology, 3D-printing, ground movements**

I. Introduction

GROUND movements usually occur in significant volumes, posing a serious and costly threat [1] which can cause irreversible damage [2], [3] and, in many cases, severe loss of life. Landslides thus can cause disastrous situations and significant casualties due to the ground displacements which arise from heavy rains, earthquakes, and even volcanic eruptions, leading to numerous fatalities and damage as has been seen in the past few decades across the globe [4]. The effects of torrential or heavy rain, coupled with wet antecedent soil moisture conditions, combine to create landslides [3], [5]. The absorbed water reduces the soil strength and increases the stress [3], making it imperative for early field monitoring, especially in the hilly areas, which are much more susceptible to landslides. This emphasizes the need for more effective, early detection of incipient soil movement, which is needed to warn about the instabilities in the condition of the slope being monitored [4], [6].

Over the past few years, new techniques for monitoring have been developed, allowing continuous measurement of ground movement [6] and thus replacing existing (and often less accurate methods) measures of ground movement. Furthermore, underground monitoring devices such as extensometers [7]–[9] can be used to monitor ground movements by correlating the change in strain observed with ground movements [7], [9] as the basis of early warning system

This work was supported by the University of Malaya through the grant UM Innovate PPSI-2020-HICOE-02 and in part by the Newton Fund Impact Scheme grant through the Newton-Ungku Omar Fund partnership under Grant IF022-2020, in part by the UK Department for Business, Energy and Industrial Strategy and Malaysian Industry-Government Group for High Technology (MIGHT). The work of K. T. V. Grattan was supported from the Royal Academy of Engineering.
(Corresponding author: Harith Ahmad).

M. A. Alias, M. F. Ismail, M. S. M. Sa'ad, M. K. A. Zaini, K. S. Lim, S. A. Reduan are with the Photonics Research Centre, University of Malaya, 50603 Kuala Lumpur, Malaysia.

K. T. V Grattan and B. M. A. Rahman are with the School of Mathematics, Computer Science & Engineering, City, University of London, London, EC1V 0HB United Kingdom.

G. Brambilla is from the Optoelectronics Research Centre, University of Southampton, Southampton SO17 1BJ, United Kingdom.

H. Ahmad is with the Photonics Research Centre, University of Malaya, Kuala Lumpur 20603, Malaysia and also with the Physics Department, Faculty of Science, University of Malaya, 50603 Kuala Lumpur, Malaysia (e-mail: harith@um.edu.my).

(EWS) performance. Existing *conventional* monitoring methods, such as electrically-based multipoint extensometers [6] and inclinometers [10], however, shows key limitations in practical usage, often critical applications, such as poor sensor stability, bulky in size, limited in-the-field durability, as well as being highly susceptible to electromagnetic interference (EMI) [10], [11]. Furthermore, given that the sites being monitored are often large and remote, the high signal loss over the long-distance transmission needed is a significant drawback in using conventional monitoring methods. Thus, this effectively prohibits the effective large-scale slope monitoring [11], [12] that is required. Another shortcoming of these traditional methods is that they do not have multiplexing capabilities that allow several sensors' interrogation in a single system.

A study by Corominas *et al.* [6] on slope monitoring has resulted in a new approach. A wire extensometer system based on the deflection of wire inside a borehole is applied to monitor surrounding ground movement, to allow the relative measurement of the positions of two chosen points. It operates as follows. First, the degree to which wire is displaced is monitored based on the electrical signals from the potentiometer that has been mounted. However, this method has the disadvantage of potential misinterpretation of the signals received due to the displacements (resulting from a landslide event) and signal interference (from any extraneous electromagnetic interference (EMI)) present, for example. Further work by Cumunel *et al.* [13] discusses using a long-gauge optical fiber extensometer system based on a method using low coherence interferometry to determine the extension of a cantilever beam. However, compensation for temperature changes is needed, but this cannot be implemented as the sensor itself and temperature compensation mechanism required cannot be in the same place – making the design unsuitable for borehole applications.

Fiber optic sensors provide a highly effective alternative to existing conventional sensors for several important reasons. They show better resistance than metallic sensors to corrosion [14], can offer higher precision, and importantly are immune to electromagnetic interference (EMI) [15]. Importantly the low loss of the fiber means that the signal integrity remains high over distances of even several kilometers – highly relevant for in-the-field monitoring conditions. Systems like this can easily be installed, and the insulator nature of the fiber itself means there is no risk of short-circuiting when used in a wet environment [11]. The Fiber Bragg Grating (FBG) can form the basis of the sensor and show advantages over conventional sensors (such as piezoelectric sensors) using not intensity but wavelength changes as the basis of the measurements [16]. FBG-based sensors had been broadly applied in a wide range of fields [17]–[19], due to being small in size, lightweight, flexible, allowing quasi-distributed monitoring and multiplexing capabilities, with continuous monitoring capabilities [20], [21] and good chemical stability [16], [22], [23]. Given these benefits, an FBG-sensor based approach to remote and automated long-distance continuous monitoring [23]–[25] has been chosen as the basis of the sensor designed in this work.

Thus, a new FBG-based extensometer system has been designed, laboratory tested, implemented, and compared to methods described in the literature, e.g., [20], [26], [27]. Table I shows the comparison between previous work and our work in terms of measurement range, responsivity, and resolution. Our proposed extensometer provides a more extensive measurement range with reasonable responsivity than the others. It also gives an alternative low cost and easy to fabricate design, taking advantage of 3D printing technology (also known as FDM technology [19], [25]). It is also crucial to provide temperature compensation for the extensometer design to ensure that it can be used effectively on site. So, an additional FBG was incorporated and characterized in a laboratory test chamber over the temperature range of 25°C to 50°C. Furthermore, the extensometer system can also be applied in various engineering applications such as structural health monitoring of bridges [28] and tunnels [29], offering a solution for structural monitoring in typical situations experienced in the field.

TABLE I
TABLE OF COMPARISON BETWEEN THE PREVIOUS WORKS AND OUR DESIGN

Ref	Measurement Range (mm)	Responsivity (nm/με)	Resolution (nm)
[20]	80	0.0065	0.05
[26]	40	0.0015	0.10
[27]	50	0.0016	0.10
This work	100	0.0012	0.02

II. EXTENSOMETER DESIGN AND OPERATION

A. Extensometer design

The FBG-based extensometer design developed in this work is shown in Fig. 1. This innovative design takes advantage, as discussed, of 3D printing technology to create a system that enables the accurate measurement of the strain variation resulting from the horizontal displacement occurring. A broad choice of filaments ('*printer inks*') is available to offer the maximum flexibility best to meet the requirements of the in-the-field applications. For example, thermoplastic polyurethane (TPU) filament is used to embed the FBGs taking advantage of its high flexibility and durability [30] to allow it to withstand much higher tensile forces, compared to other standard filaments such as those using polylactic acid (PLA) and acrylonitrile butadiene styrene (ABS) [31]. A further reason for the choice of TPU is its high strain sensitivity (among other filaments), making it well suited to use on pipes or cylindrical structures [23], [32]. Furthermore, rigid filaments (made of PLA) are well suited to the design of the temperature compensation in the sensor system, taking advantage of its hardness [30], as well as the ease of setup of the system and printing [15].

To construct the sensor system from the various 3D printed components, the commercial adhesive could then be applied to bond the FBG and the inner walls of both the TPU and the PLA materials, taking advantage of their ability to function well over a wide range of temperatures [33]. A PVC pipe was chosen as the extensometer body. Published work [34], [35] had shown

that polyvinyl chloride (PVC) pipes are good to use for bending applications taking advantage of their flexibility, lightweight, and ease of installation, compared to metallic pipes [34]. PVC pipes can also sustain more significant tensile stress without failing [36], necessary for strain measurements and ease of construction. In addition, the commercial protective tape can be used to seal and bond the sensors to the extensometer body for use even below ground level, without this affecting its performance. The system was packaged in a way that makes it well suited to in-the-field applications, for the extensometer to operate efficiently and reliably, a protective nylon cloth (and adhesive tape) was used as reinforcement on the extensometer to ensure a smooth finish [1] and to prevent ingress of moisture from the soil [35], especially during installation.

As shown in Fig. 1, the extensometer system was fixed rigidly at two points, allowing any strain occurring between those two points to be measured, and the data collected then analyzed. When placed in a vertical position (as is the case for underground use), the extensometer will inevitably be influenced by the soil surrounding it. Due to gravity, this will affect the extensometer structure by causing a displacement along its length.

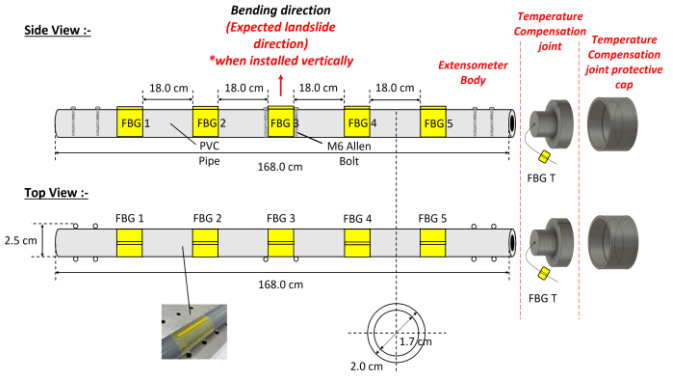

Fig. 1. Illustration of the design of the FBG-based extensometer system, showing the strain sensitive FBGs (FBG1,2….5) written onto the optical fiber used and also on the temperature compensator (FBG T) placed at the joint and cap

B. FBG-based strain sensor

A schematic diagram of the embedded FBG-based strain sensor is shown in Fig. 2 where the sensor was fabricated with 3D printing technology, using the TPU filament material. The sensor element (FBG 1, 2 ….5 from Fig. 1) was cuboid-shaped with the FBG embedded inside of dimensions of 40 x 1.2 x 1.2 mm and an infill density of 20 %. Furthermore, as shown in Fig. 2, the sensor has been designed with a thin base (or brim) to allow better adhesion to the extensometer structure. The FBG was pre-stressed before the gluing process using cyanoacrylate glue to bond the FBG to its position inside the printed holes (1.2 mm x 1.2mm), where the pre-stressing was applied by pulling the end of the fiber containing the FBGs, noting that it was taped to stop the fiber from moving before the gluing process was carried out.

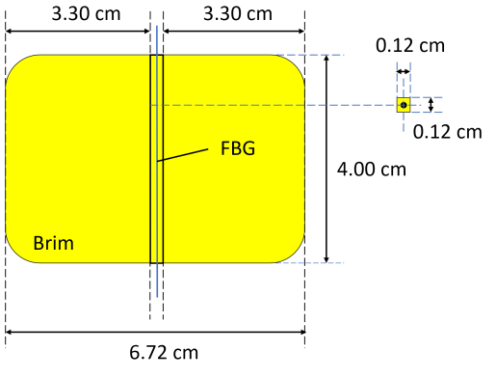

Fig. 2. Illustration of the dimensions of the embedded FBG-based strain sensor (as stated) used in the extensometer system

C. Temperature compensation (through the FBG T) integrated with the joint and joint cap

As can be seen from the figure, a further FBG (denoted as FBG T) has been incorporated in this extensometer system to provide an effective temperature compensation mechanism. This FBG was fixed in a casing to protect the FBG T (as shown in Figure 3, also termed the 'FBG T joint') to maintain the integrity of the system. Fig. 3(a) shows details of the FBG T joint, which was 3D printed using the PLA filament and then placed at the rigid points and thus free from any strain at each end of the extensometer. The optical fiber was then inserted through the holes in the FBG T joint, as shown in the figure, and the FBG T was left loose inside the pipe so that it was not subject to strain effects and could be used to measure temperature changes alone. Finally, a cover was fabricated to seal the joint and thus protect the FBG T to enable it to be used effectively in the field. The dimensions of the design used in this work are illustrated in Fig. 3(b).

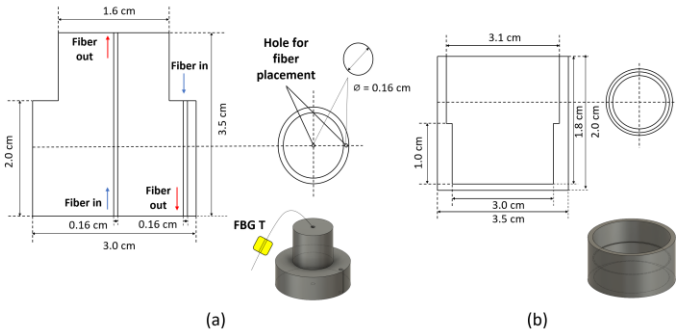

Fig. 3. Illustration of (a) the temperature compensation joint (containing the temperature compensating FBG element FBG T) and (b) its protective joint cap, showing also the dimensions used

D. Design principles for the FBG-based extensometer system

The FBG-based strain sensors attached to the body of the extensometer were created by embedding an optical fiber, containing the in-fiber written FBGs, inside a 3D printed structure (TPU), (with dimensions as stated in Fig. 2), where, as indicated before, FBG acts as a wavelength-selective device. Noting that changes in the surrounding temperature affect the Bragg wavelength due to the thermal expansion or contraction of the grating periodicity, in most practical applications, the Bragg wavelength shift of FBGs ($\Delta\lambda_b$), can be written as in Eq. (1)[4], [30]:

$$\frac{\Delta\lambda_b}{\lambda_b} = \left(1 - p_{eff}\right)\Delta\varepsilon + (\alpha + \xi)\Delta T \quad (1)$$

where p_{eff} represents the photo-elastic parameter of the material, $\Delta\varepsilon$ the strain changes experienced, α is the coefficient of thermal expansion of the fiber material, ξ is the thermo-optic coefficient of the fiber, and ΔT is the temperature change experienced. The use of an unstrained FBG (where $\Delta\varepsilon$ = 0 in Eq. (1)) is used to provide temperature compensation (as seen in FBG T) for the determination of the temperature effect alone and thus to compensate for it and allow the strain effect alone on each FBG used to be determined.

In this work, the different FBG strain sensors incorporated were attached to a PVC pipe which formed the body of the extensometer, as shown schematically in Figs. 4(a) and (b). The displacement curve, v(x), can be derived through the curvature function, K(x), based on the geometric relationship of the curvature and displacement of the span of the device. Assuming the displacement is small, the curvature and vertical displacement are given by Yau *et al.* [28], based on the similar mathematics seen for a bridge structure, where:

$$K = \frac{d^2v}{dx^2} \quad (2)$$

giving,

$$v = \iint K\, dxdx \quad (3)$$
$$v = K \iint dxdx \quad (4)$$

The correlation between the strain, ε, and the curvature, K, of the extensometer is given by:

$$K = \frac{\varepsilon_n}{y} \quad (5)$$

where n is the n^{th} longitudinal location of strain measured and y is the distance from the neutral axis of the cross-section. For two sensors placed on the top and bottom of the structure under investigation, at corresponding longitudinal locations the curvature K can be expressed as

$$K = \frac{\varepsilon_b - \varepsilon_t}{h} \quad (6)$$

where h is the distance between the FBG sensors, ε_b and ε_t are the strain measured at the bottom and at the top of the structure, respectively. Since the strain was only measured at the bottom, ε_t was considered to be zero (ε_t= 0). When measuring the vertical displacements of the extensometer in real-time, the curvature curve can be assumed to be a quadratic equation:

$$K(x_n) = ax_n^2 + bx_n + c \quad (7)$$

where a, b and c are unknown constants and determined by the least square method. The displacement curve can then be determined by performing a double integration in which Eq. (7) is substituted into Eq. (3) to give,

$$v(x) = \iint (ax_n^2 + bx_n + c)\, dxdx \quad (8)$$
$$v(x) = \frac{ax^4}{12} + \frac{bx^3}{6} + \frac{cx^2}{2} + dx + e \quad (9)$$

where d and e are integration constants that can be obtained by applying the boundary conditions: zero displacements occur at the fixed ends of the extensometer (these are rigid points). This condition can be represented mathematically as $v(0)$ = 0 and v(L) = 0, where L is the span length of the extensometer, giving e = 0 and

$$d = -\left(\frac{aL^3}{12} + \frac{bL^2}{6} + \frac{cL}{2}\right) \quad (10)$$

Substituting Eq. (10) into Eq. (9), the displacement function can then be determined as

$$v(x) = \frac{ax^4}{12} + \frac{bx^3}{6} + \frac{cx^2}{2} - \left(\frac{aL^3}{12} + \frac{bL^2}{6} + \frac{cL}{2}\right)x \quad (11)$$

The temperature compensating grating, FBG T, was installed to eliminate any temperature cross-sensitivity in strain measurements.

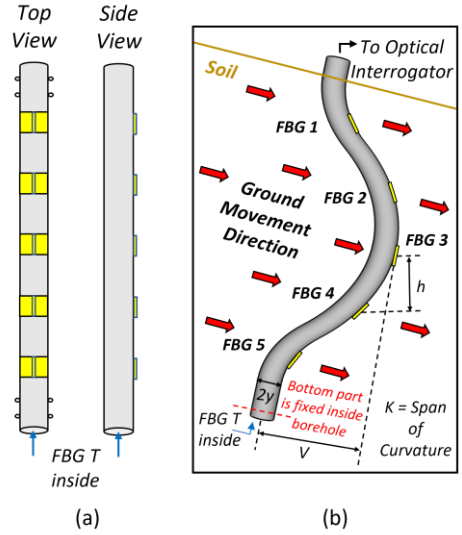

Fig. 4. Illustration of (a) top and side view of extensometer (without the protective layer) and (b) the working principle of the FBG-based strain sensor installed on the PVC pipe (extensometer body)

III. Laboratory-based Calibration of the Sensor System

A. Comparison of protected and unprotected FBG sensors

The experimental setup used to allow a comparison of the performance of both 'protected' and 'unprotected' FBG sensors is illustrated in Fig. 5(a). The type of FBG used is the uniform positive-only index change. Here the aim is to evaluate if the performance of the sensor system was affected by the tape used to protect it from the environment. Photographs of the two setups are shown in Fig. 5(b). In the 'protected' arrangement, self-fusing silicon rubber tape was chosen for its outstanding characteristics, as it has excellent moisture and waterproofing properties and is highly flexible and is long-lasting at extreme temperatures (-60°C to +200°C) – all this making it very well suited for sealing materials below ground level. Thus, after sealing the FBG-based strain sensor system with protective tape (silicon self-fusing tape) to create the 'protected' sensor set up,

the performance of the FBG strain sensor could then be evaluated, also allowing a comparison between the 'protected' and unprotected' setups. Fig. 5 shows one of the FBG-based strain sensors (of dimensions as stated in Fig. 2) attached to one side of the PVC pipe (the 'tensile side') at the zero displacement point – this was used to acquire the initial spectrum of the 'unprotected' FBGs. Then, at the bending point (which was 82.0 cm from the zero displacement point in a pipe of length 168 cm), the PVC pipe was displaced horizontally, at intervals of 2.5 cm, from zero to 10.0 cm, noting the shift in the reflective wavelength of the FBGs. Here the aim is to evaluate if the performance of the sensor system was affected by the tape used to protect it from the environment. Photographs of the two setups are shown in Fig. 5(b). In the 'protected' arrangement, self-fusing silicon rubber tape was chosen for its outstanding characteristics, as it has excellent moisture and waterproofing properties and is highly flexible and is long-lasting at extreme temperatures (-60°C to +200°C) – all this making it very well suited for sealing materials below ground level. Thus after sealing the FBG-based strain sensor system with protective tape (silicon self-fusing tape) to create the 'protected' sensor set up, the performance of the FBG strain sensor could then be evaluated, also allowing a comparison between the 'protected' and unprotected' setups. Fig. 5 shows one of the FBG-based strain sensors (of dimensions as stated in Fig. 2) attached to one side of the PVC pipe (the 'tensile side') at the zero displacement point – this was used to acquire the initial spectrum of the 'unprotected' FBGs. Then, at the bending point (which was 82.0 cm from the zero displacement point in a pipe of length 168 cm), the PVC pipe was displaced horizontally, at intervals of 2.5 cm, from zero to 10.0 cm, noting the shift in the reflective wavelength of the FBGs.

Measurements on these two different setups were then repeated, and results were compared. The response of the FBGs used was observed using a Yokogawa AQ6370C (600 nm – 1700 nm) optical spectral analyzer. Fig. 5(c) illustrates a representative output optical spectrum (of one of the FBG-based strain sensors with a reflective wavelength of 1550.52 nm before and after the protective tape was applied to hold the sensor firmly). A slight initial wavelength shift of 0.122 nm was detected when the protective tape was used to seal the FBG strain sensor due to the strain that process applied to the sensor, shifting the 'zero point' of the calibration. The responses of both the 'protected' and 'unprotected' strain sensors to strain variations at positions 0 to 10cm were evaluated, and the results are presented in Fig. 5(d). It can be seen that the 'protected' sensor performance showed a sensitivity that was ~1.13 times higher than that for the 'unprotected' sensor. Still, more importantly, the key benefit of using this tape was its long-lasting, anti-moisture, and excellent waterproof properties. For many planned applications, the relatively air-tight sealing, the ability to withstand an operating temperature range of -60°C to +200°C, and resistance to water and moisture are important advantages. In this way, it creates the basis of a practical sensor for use in the field, especially in underground environments, reliable for ground movement monitoring and operating under various extremes of the possible weather conditions.

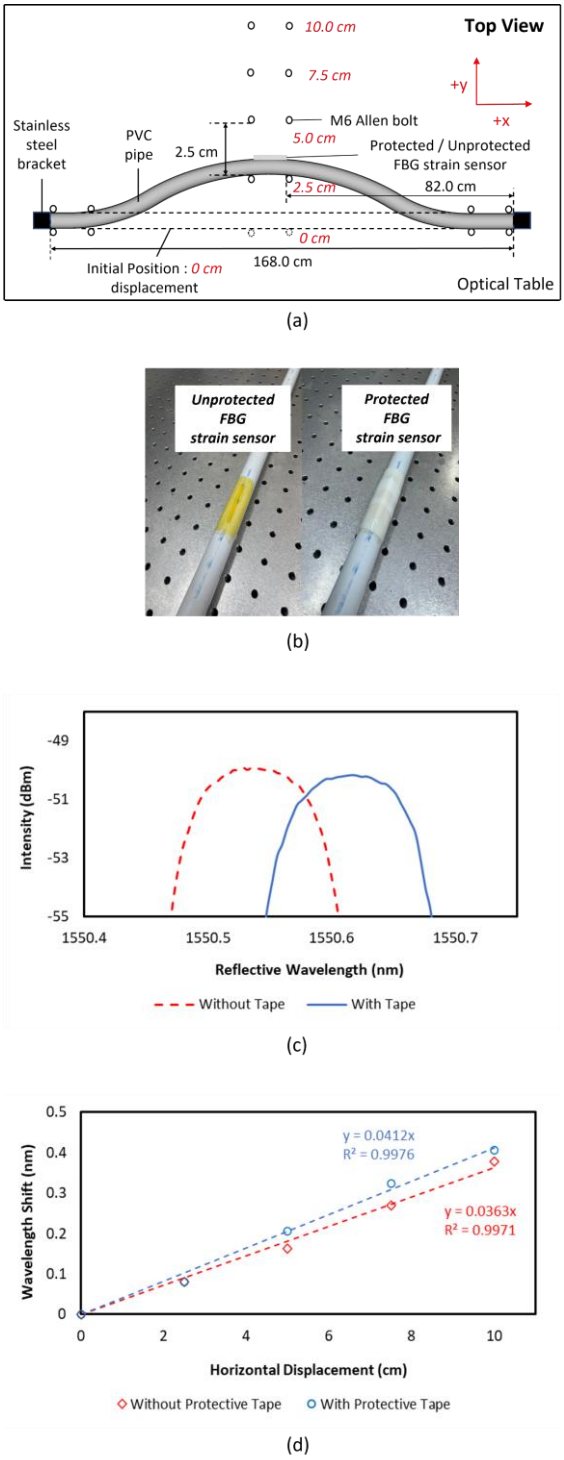

Fig. 5. Illustration of (a) the experimental setup for the protected and unprotected FBG-based strain sensor measurements, (b) comparison (actual picture) of both unprotected and protected FBG strain sensor, (c) the spectrum of 'unprotected' strain sensor (red dots) and the 'protected' strain sensor (solid blue line) and (d) linear fit of the calibration of both 'unprotected' (red) and 'protected' (blue) strain sensor.

B. *Experimental strain measurements – System set up*

Taking advantage of the superior performance of the 'protected' sensor arrangement, the experimental setup used to evaluate the FBG-based extensometer based on it is presented in Fig. 6(a). Here, the strain monitored arises from the

horizontal displacement of the PVC pipe along with the optical table, where the strain was monitored. The PVC pipe was first laid horizontally on the optical table (equipped with a rectangular grid of tapped M6 holes) to conduct a preliminary laboratory evaluation. Then, both ends of the PVC pipe were fixed with a stainless-steel bracket and four identical (M6-type) Allen bolts (with two on each side) to prevent the PVC pipe from rotating during the experiment. Next, the five FBGs (each of different reflective wavelengths labelled as FBG 1 to FBG 5) which form the sensor system were used and incorporated to form the basis of the different measurement points considered along the extensometer length (with FBG T used for temperature compensation). Next, the FBGs were evenly distributed on the outer layer of the PVC pipe (tensile side, assuming that the ground moves in this direction) to evaluate the sensor performance, monitoring strain variations along the horizontal axis. All six FBGs (FBG 1, FBG 2, FBG 3, FBG 4, FBG5, and FBG T) were spliced together (Table II shows these FBGs and their respective reflective wavelengths used in the extensometer) in series along with a single optical fiber and placed on one side of the pipe (with FBG T placed loose inside the pipe to keep it insensitive to strain).

A schematic diagram of the interrogation system used is presented in Fig. 6(b). Here an amplified spontaneous emission (ASE) light source was connected to Port-1 of a 3-port circulator. The optical fiber with the serially-spliced FBGs was connected to Port-2, while its response was observed using a Yokogawa AQ6370C (600 nm–1700 nm) optical spectral analyzer (OSA), which was connected to Port-3. The responses and thus reliability of each FBGs used for strain measurements except for FBG T were obtained, based on the horizontal displacement at the mid-length of the pipe at the bending point, monitored on the optical table. The position of each FBG strain sensor used and the bending direction of the pipe is shown in Fig. 6(a). As the PVC pipe was bent towards the bending direction, all the FBGs except FBG T, unaffected by strain variations, would experience tensile strain. Their response was measured at 2.5 cm intervals, ranging from 0 to 10 cm. According to Hooke's Law, a linear correlation between the strain and stress of the pipe would be expected (only until the yield point where the pipe would be permanently deformed or even broken).

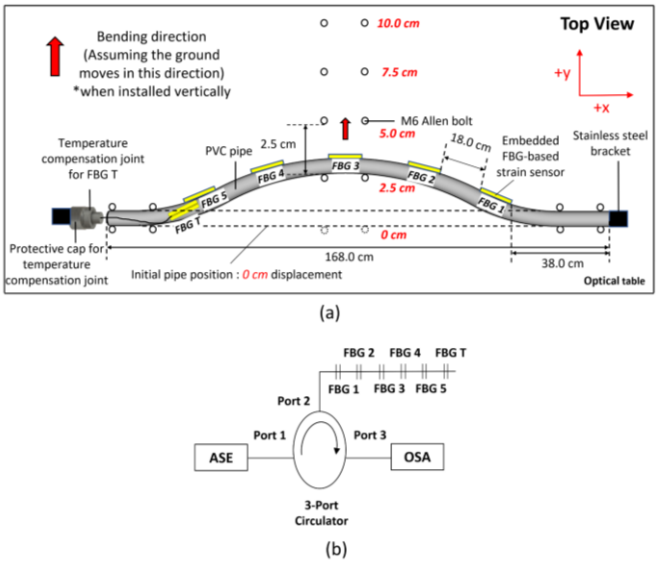

Fig. 6. Illustration of (a) the top view of the experimental setup of the FBG-based extensometer and (b) schematic diagram of interrogation system for the FBGs used (FBG 1 to FBG 5) and FBG T.

TABLE II
FBG POSITIONS AND THEIR RESPECTIVE REFLECTIVE WAVELENGTHS USED IN THE EXTENSOMETER

FBG #	Reflective wavelength (nm)	Position along the pipe (cm)	Condition
1	1557.5	41.0	Tensile Strain
2	1555.1	63.0	Tensile Strain
3	1552.5	85.0	Tensile Strain
4	1550.3	107.0	Tensile Strain
5	1546.0	129.0	Tensile Strain
T	1540.0	Inside the pipe	Loose

C. Setup for field testing

Good packaging and protection in below-ground environments are needed to ensure efficient and reliable extensometer performance during field testing. A protective nylon cloth was wound around the extensometer body to provide waterproofing to protect the system further, as shown in Fig.7 (a). Then, an additional layer of the black plastic sheet was applied on the outer part of the extensometer body (shown in Fig.7 (b)) to provide a smoother surface during installation and conserve the soil moisture during testing. To determine the exact location of each strain-sensitive FBG sensor (FBG 1, FBG 2, FBG 3, FBG 4, and FBG 5) during installation, a cloth

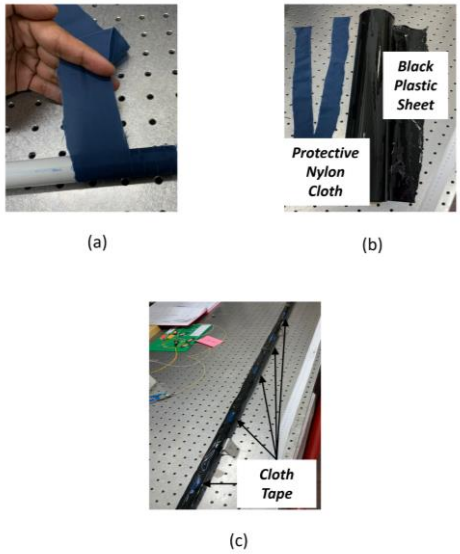

Fig. 7. Illustration of (a) the winding scheme of protective nylon cloth, (b) actual picture of black plastic sheet and protective nylon cloth, and (c) the placement of cloth tape at the opposite side of all strain-sensitive FBG sensors

tape was used and pasted on top of the black plastic sheet on the opposite side of each FBG sensors, as illustrated by Fig.7 (c).

The setup used to evaluate the extensometer response during the field test is presented in Fig. 8(a), illustrating that the system allows the bending of the extensometer to be associated with soil movements simulated by applying known forces (from weights), which causes strain variations that can readily be monitored. First, the extensometer was suspended in the middle of the container (of dimensions of 175 cm x 50 cm x 50 cm, and 25 cm from the bottom) using two PLA-based 3D Printed extensometer holders (screwed into the wood), which provides rigid points at both ends. Then, each end of the extensometer was taped tightly with the extensometer holder, using cloth tape to prohibit any form of rotation from occurring during testing. Next, the exact location of each FBG sensor was marked on the cloth tape, as shown in Fig. 8(b), following which the extensometer was buried 10 cm underground (where the ground level was monitored using a measuring tape attached to the inner walls of the wooden box).

Fig. 6(b) shows the optical interrogation setup, with an amplified spontaneous emission light source used at Port-1 of the 3-port circulator. The serially-spliced FBGs were located on the extensometer body connected to Port-2. In contrast, Port-3 was connected to a Yokogawa AQ6370C (600 nm–1700 nm) Optical Spectrum Analyzer (OSA) to measure the response of the FBGs to the applied forces using weights ranging from 1 kg to 10 kg placed directly on the soil above each strain-sensitive FBG location. It is illustrated in Fig. 8(b), and the earth can move downwards under gravity.

Using this setup, the response of the extensometer was first measured in *dry soil*, with weights increased in 1kg intervals over the range from 1 kg to 10 kg, which was initially applied to FBG 1. Then, the same steps were repeated for FBG 2, FBG 3, FBG 4, and FBG 5, except for FBG T, inside the extensometer body. The experiment was then repeated with wet soil, using 10 kg in water mass, applying the forces, in the same way, to enable a close comparison of the system's performance under these different conditions.

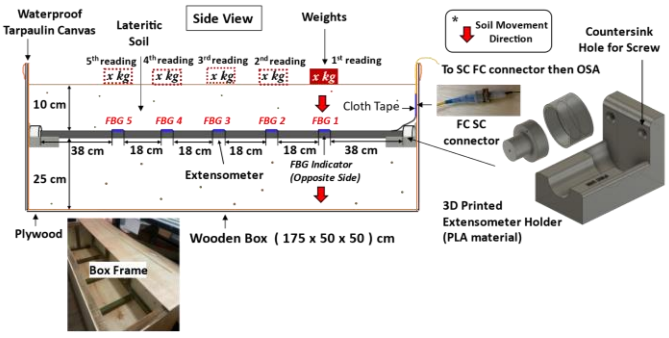

(a)

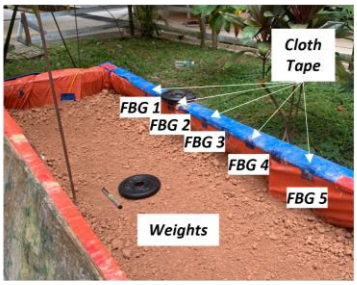

(b)

Fig. 8. Illustration of (a) the field-testing setup for the FBG-based extensometer and (b) picture of field testing taking place

D. Temperature Characterization

Temperature characterization on FBG T had also been carried out by placing the FBG sensor inside a water bath to be calibrated. To undertake this, the temperature inside the water bath was initially set at 25°C (room temperature) and was increased gradually (in 5°C intervals) until it reaches 50°C. At the same time, the wavelength shift of FBG T was observed and recorded.

IV. Results and Discussion

A. Strain measurements using the FBG-based extensometer system

Fig. 9 shows the reflection spectra of the series of FBGs used in the optical fiber network forming the extensometer system. Tests were carried out when the mid-length of the extensometer was pushed towards the positive y-axis direction, as shown in the setup in Fig. 6(a) – this direction (positive y-axis) is perpendicular to the whole extensometer length on the x-axis. These results obtained from the tests show that the reflective wavelengths of FBG 1 to FBG 5 experience a redshift at different values, as their horizontal displacement changes from the initial point to 10 cm (in 2.5 cm increments). For example, Fig. 9 illustrates that FBG 3 experiences the most significant spectral redshift. It is because this FBG was placed directly at the extensometer body's bending point, which was also the furthest from the two rigid points. As expected, FBG 1 and FBG 5 experience the least spectral redshifts compared to the other FBGs, as they are positioned nearer to the fixed points.

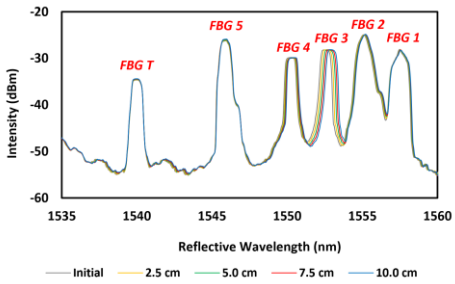

Fig. 9. The wavelength spectra of all FBGs at different horizontal displacements (from 0 to 10 cm, in increments of 2.5 cm)

The effect is shown in Fig. 9, illustrating that FBG3 shows the maximum displacement compared to the other FBGs closer to the rigid points. Fig. 10 provides the calibration of the extensometer performance. Fig. 10(a) shows the wavelength shifts in nm for all the five FBGs as they experience strain variations in response to increasing horizontal displacement. The wavelength shift of each FBG is different due to the positions of the FBGs (and given by $\Delta\lambda_{FBGn}$ (where n = 1, 2 … 5), such that $\Delta\lambda_{FBG\,3} > \Delta\lambda_{FBG\,2}$ & $\Delta\lambda_{FBG\,4} > \Delta\lambda_{FBG\,1}$ & $\Delta\lambda_{FBG\,5}$). Fig. 10(b) presents the strain profile of the whole extensometer system with increasing horizontal displacement with respect to the positive y-axis direction from

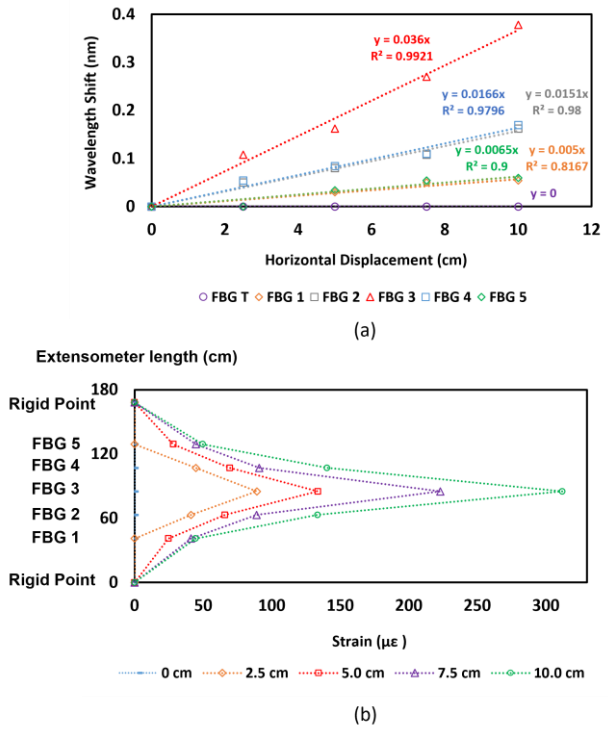

Fig. 10. Illustration of the of the (a) wavelength shift of all FBGs experiencing strain variations in response to increasing horizontal displacement towards the positive y-axis direction and (b) strain profile of whole extensometer system with increasing horizontal displacement towards the positive y-axis direction (0cm to 10cm).

0 cm to 10 cm in 2.5 cm increments, illustrating the system's good performance overall.

The responsivities of each strain-sensitive FBGs with the horizontal displacement are presented in Table III, confirming the excellent linear fit seen in Fig. 10 with an average responsivity of 0.0158 nm/cm, and as expected with each FBG showing a different degree of wavelength shift due to their different positions on the extensometer body as given in Fig. 6(a). Overall, a very satisfactory linear fit is observed, with an excellent average R^2 value of 0.87, providing confidence in using the extensometer system in practice.

TABLE III
RESPONSIVITY OF EACH STRAIN SENSITIVE FBG (N = 1……5) TO STRAIN VARIATION

FBG #	Responsivity (nm/cm)	R^2
1	0.0050	0.8167
2	0.0151	0.9800
3	0.0360	0.9921
4	0.0166	0.9796
5	0.0065	0.9000

B. Field testing of the extensometer in both dry and wet soil

The setup shown in Fig. 8 was used to evaluate the extensometer system in both dry and wet soil. To do so, firstly, the wavelength shifts of several FBGs, FBG T and FBG 4, these being a strain insensitive FBG and a strain sensitive FBG, respectively, in the optical fiber network before and after being buried underground, were obtained and are shown in Fig. 11. From Fig. 11(b), it can be seen that FBG 4 experiences a blueshift of 0.24 nm, indicating that it is shifted to the left after being buried, which aligns well with the average wavelength shift for all strain-sensitive FBGs of 0.24 nm. Furthermore, the blueshift experienced also shows a decrease in surrounding temperature after being buried, causing the gratings of the strain-sensitive FBGs to experience both temperature and strain changes.

In order to allow the temperature effects to be corrected, the wavelength shift for all strain-sensitive FBGs was subtracted from the data obtained in Fig. 11(a), showing that FBG T was shifted to the left by 0.16 nm after being buried. Accurate strain measurement can be obtained from the strain-sensitive sensors by subtracting off with 0.16 nm from the data obtained in FBG

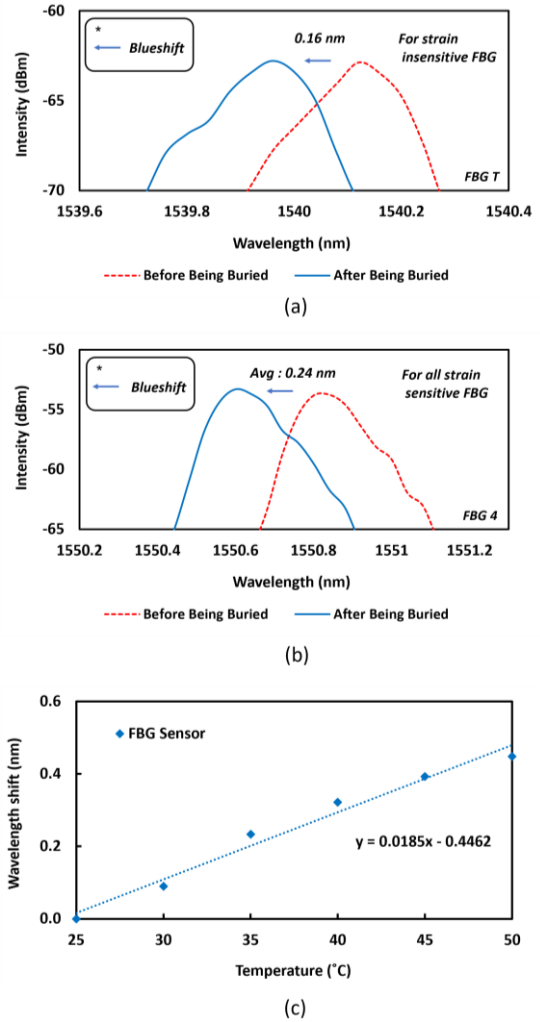

Fig. 11. Illustration of the wavelength shift of FBG T (strain insensitive FBG) and (b) FBG 4 (example of strain sensitive FBG) before and after being buried underground and (c) temperature sensitivity of FBG T

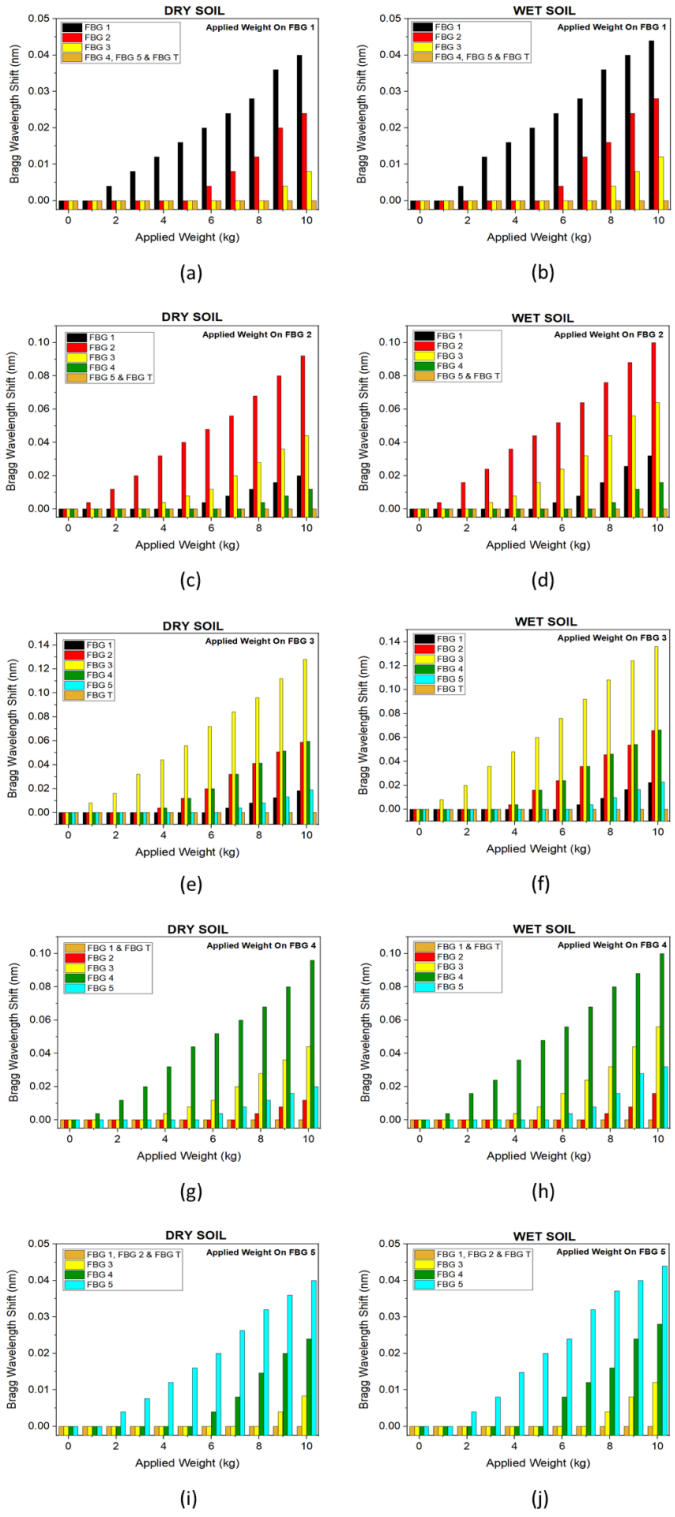

Fig. 12. Illustration of (a) the wavelength shift (nm) of all FBGs in response to increasing applied weights (kg) on FBG1 in dry soil and (b) wet soil, (c) the wavelength shift (nm) of all FBGs in response to increasing applied weights (kg) on FBG2 in dry soil and (d) wet soil, (e) the wavelength shift (nm) of all FBGs in response to increasing applied weights (kg) on FBG3 in dry soil and (f) wet soil, (g) the wavelength shift (nm) of all FBGs in response to increasing applied weights (kg) on FBG4 in dry soil and (h) wet soil, (i) the wavelength shift (nm) of all FBGs in response to increasing applied weights (kg) on FBG5 in dry soil and (j) wet soil.

T. This is also due to the gratings of FBG T experiencing only temperature changes as a result of a decrease in surrounding temperature, thus, making it suitable as a temperature sensor to provide compensation. The temperature sensitivity of FBG T was shown in Fig. 11 (c), where it is monitored to be 18.5 pm/°C.Fig. 12 shows data on the field testing when the weights are applied, with separate bar graphs showing the wavelength shift of each extensometer FBG in both dry and wet soil. Fig. 12(a) shows the effect in dry soil on FBG 1, showing the differences in the wavelength shifts of each strain-sensitive FBG, and Fig. 12 (b) shows a similar calibration graph for wet soil when weights are applied to FBG 1. Fig. 12(c),(d),(e),(f),(g),(h),(i), and (j) provides the detailed calibration data when weights were applied to each FBG location, inducing strain with the difference in wavelength shifts being due to the movement of soil acting upon each FBG forming the sensor system.

Figure 12 illustrates that the FBGs showing the highest wavelength shift are those where the highest strain has been induced and which experience the highest weights applied – for instance, from Fig. 12(a), FBG 1 shows the highest wavelength shift followed by FBG 2 and FBG 3, while FBG 4, FBG 5, and FBG T showed no responses, as the distance of each FBGs from the rigid point significantly affects its response. For example, Fig 12(c) shows that the wavelength shift of FBG 1 is higher than FBG 4 but lower than FBG 3 when FBG 2 was strained

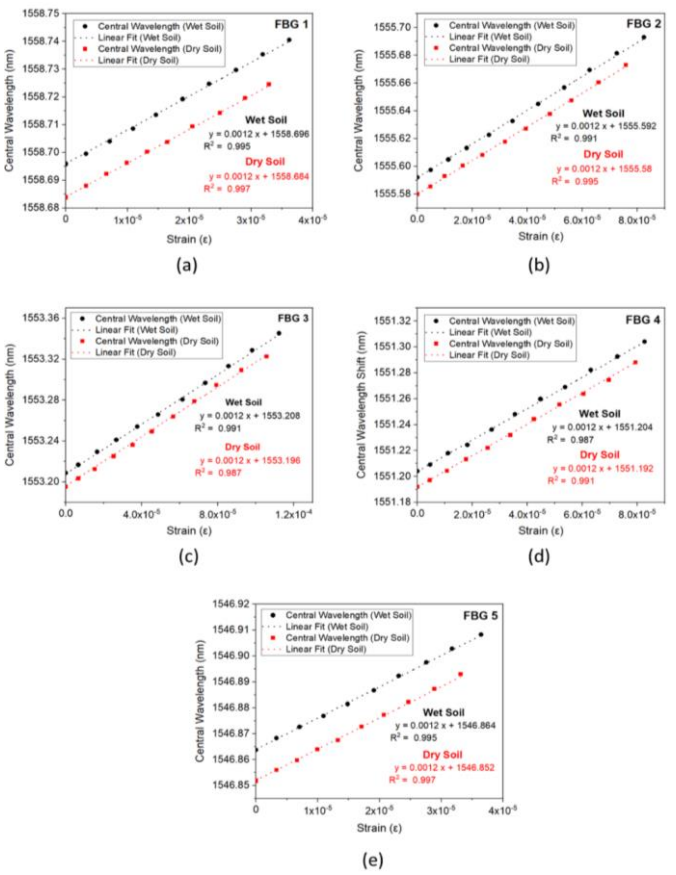

Fig. 13. Illustration of the calibration graphs (in both dry (in red) and wet (in black) conditions) of (a) FBG 1, (b) FBG 2, (c) FBG 3, (d) FBG 4 and (e) FBG 5.

because FBG 1 is closer to the rigid point than FBG 3. The calibration also shows that the wavelength shifts of all the FBGs forming the extensometer system were also higher in wet soil than in dry soil conditions. Fig. 13 shows the calibration graphs of all the strain-sensitive FBGs under both dry and wet soil conditions. Fig. 13(a) shows the wavelength shift of FBG 1 to increasing strain due to applying weights above the location of FBG 1 in both dry and wet soil. A similar approach was applied to the other FBGs, FBG 2, FBG 3, FBG 4, and FBG 5, and the calibrations from these are given in Figs. 13(c), (d), (e), and (f)

The responsivities of all the strain-sensitive FBGs with respect to varying applied weights are similar in dry and wet soil conditions, giving an average wavelength responsivity of 0.0012 nm/με. However, the central wavelength shift of all the FBGs studied in damp soil was higher, as they experience a higher strain variation than under dry soil conditions. In addition, a slight shift in the initial central wavelength of all the FBGs used (~0.01 nm) was due to the wet soil being slightly heavier than the dry soil. Fig. 14 illustrates this for all the FBGs under both types of conditions.

Fig. 14 shows several graphs of the strain profile in response to various strains resulting from weights applied to several respective FBG locations. FBG 3 shows the most significant effect as it is located at the bending point of the extensometer body and thus furthest from the rigid points, compared to FBG 1 and FBG 5, closer to the fixed points. This also explains why no strain was recorded for FBG 4 and FBG 5 when weight was applied to FBG 1 as it was further away from the applied weight. The same argument applied when the weight was placed on FBG 5, and thus no strain was detected from FBG 1 and FBG 2. In wet soil conditions, muddy and less solid than dry soil, the strain profile was more significant due to the greater bending of the extensometer.

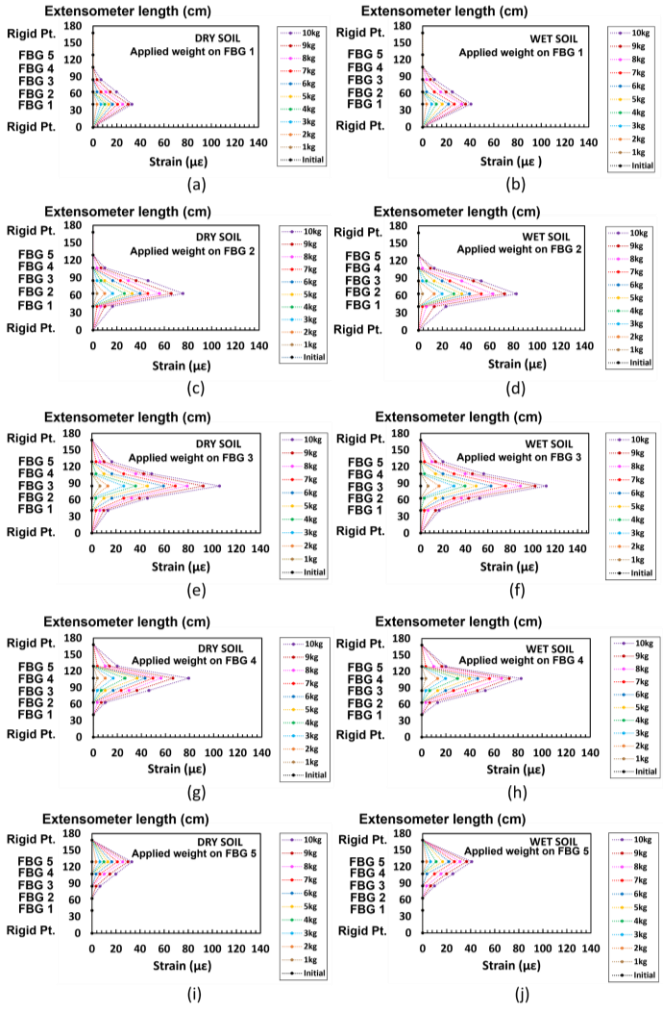

Fig. 14. Illustration of (a) the strain profile of the extensometer in response to increasing applied weights (kg) on FBG1 in dry soil and (b) wet soil, (c) the strain profile of the extensometer in response to increasing applied weights (kg) on FBG2 in dry soil and (d) wet soil, (e) the strain profile of the extensometer in response to increasing applied weights (kg) on FBG3 in dry soil and (f) wet soil, (g) the strain profile of the extensometer in response to increasing applied weights (kg) on FBG4 in dry soil and (h) wet soil, (i) the strain profile of the extensometer in response to increasing applied weights (kg) on FBG5 in dry and (j) wet soil.

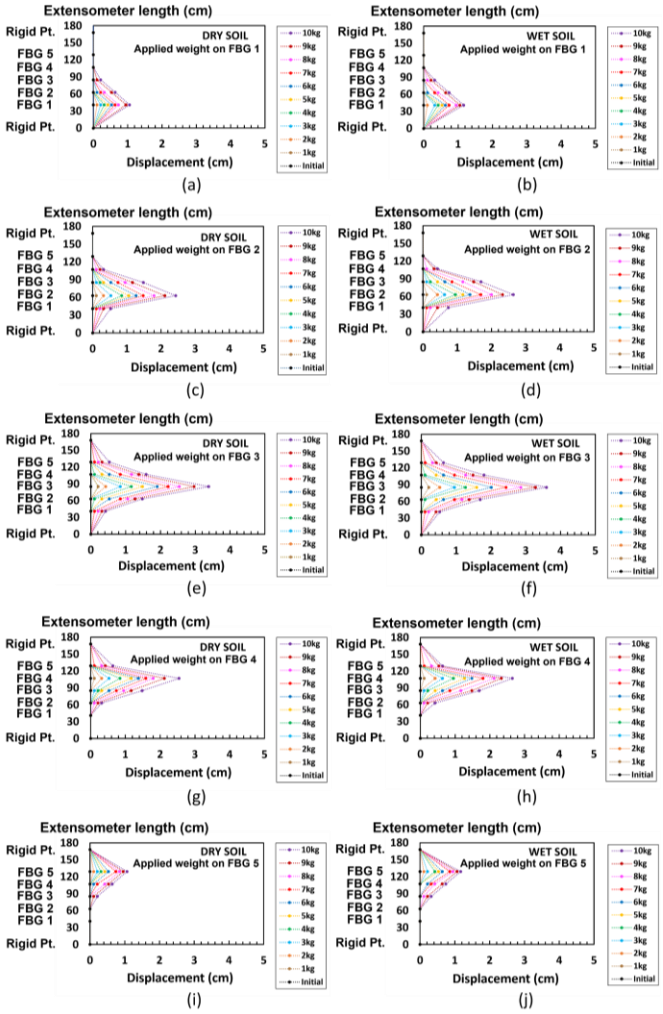

Fig. 15. Illustration of (a) the displacement of the extensometer in response to increasing applied weights (kg) on FBG1 in dry soil and (b) wet soil, (c) the displacement of the extensometer in response to increasing applied weights (kg) on FBG2 in dry soil and (d) wet soil, (e) the displacement of the extensometer in response to increasing applied weights (kg) on FBG3 in dry soil and (f) wet soil, (g) the displacement of the extensometer in response to increasing applied weights (kg) on FBG4 in dry soil and (h) wet soil, (i) the displacement of the extensometer in response to increasing applied weights (kg) on FBG5 in dry soil and (j) wet soil.

Fig. 15 illustrates the displacement of the extensometer in response to increasing applied weights on the different FBGs, in both dry and wet soil. Fig. 8(a) shows the extensometer placement inside the wooden box – it can be seen that it causes it to bend downwards from its initial position when weights are applied to each FBG location. Fig. 15 illustrated the FBG response when the extensometer was bent downwards due to the range of weights applied (in 1kg increments) to respective FBG locations. A similar trend can be seen with the graphs in Fig. 14, responding to Eqs. (4) and (7) show that displacement is linearly related to changes in strain applied.

V. Conclusion

In this work, the construction of an FBG-based extensometer that has been shown to monitor lateral ground movements effectively was designed around a series of FBG-based strain sensors and fabricated simply and inexpensively using the 3D-printing technique reported. The results obtained have shown an average grating responsivity of 0.0158 nm per cm displacement and high linearity of up to 99%, with a linear trend. Furthermore, the design was robust and based around a strain sensor with a series of protected FBGs, using waterproof tape and showing that this provides excellent waterproofing properties over the operating temperature range studied.

Field testing has illustrated the system reliability under operational conditions, with FBGs showing a responsivity of 0.0012 nm/με, in dry and wet soil conditions with response to increasing applied strains, with high linearity of up to 99%. The work done shows that the extensometer system was reliable and easy to use for continuous ground monitoring, vital for flood mitigation purposes. The next stage of the work will evaluate actual earthwork slopes to show that the results obtained have broad applicability for geotechnical engineers.

Acknowledgment

This work was supported by a Newton Fund Impact Scheme grant, ID IF022-2020, under the Newton-Ungku Omar Fund partnership. The grant is funded by the UK Department for Business, Energy and Industrial Strategy and Malaysian Industry-Government Group for High Technology (MIGHT). This work was also supported by the University of Malaya under the grant UM Innovate PPSI-2020-HICOE-02. Grattan also acknowledges the support from the Royal Academy of Engineering.

References

[1] Q. Zhang, Y. Wang, Y. Sun, and L. Gao, "Using custom fiber Bragg grating-based sensors to monitor artificial landslides," *Journal of Sensors*, vol. 16, no. 9, pp. 1–13, 2016, doi: 10.3390/s16091417.

[2] Y. Zheng, Z. W. Zhu, and Q. X. Deng, "Theoretical and experimental study on the fiber Bragg grating-based inclinometer for slope displacement monitoring," *Optical Fiber Technology*, vol. 49, no. 18, pp. 28–36, 2019, doi: 10.1016/j.yofte.2019.01.031.

[3] R. L. Ray and F. de Smedt, "Slope stability analysis on a regional scale using GIS: A case study from Dhading, Nepal," *Environmental Geology*, vol. 57, no. 7, pp. 1603–1611, 2009, doi: 10.1007/s00254-008-1435-5.

[4] Y. Hu, C. Hong, Y. Zhang, and G. Li, "A monitoring and warning system for expressway slopes using FBG sensing technology," *International Journal of Distributed Sensor Networks*, vol. 14, no. 5, 2018, doi: 10.1177/1550147718776228.

[5] R. L. Ray and J. M. Jacobs, "Relationships among remotely sensed soil moisture, precipitation and landslide events," *Natural Hazards Journal*, vol. 43, no. 2, pp. 211–222, 2007, doi: 10.1007/s11069-006-9095-9.

[6] J. Corominas, J. Moya, and A. Lloret, "Measurement of landslide displacements using a wire extensometer," *Engineering Geology*, vol. 55, no. 3, pp. 149–166, 2000, doi: 10.1016/S0013-7952(99)00086-1.

[7] H. Sanada, Y. Sugita, and Y. Kashiwai, "Development of a multi-interval displacement sensor using fiber Bragg grating technology," *International Journal of Rock Mechanics and Mining Sciences*, vol. 54, pp. 27–36, 2012, doi: 10.1016/j.ijrmms.2012.05.020.

[8] E. Intrieri, G. Gigli, F. Mugnai, R. Fanti, and N. Casagli, "Design and implementation of a landslide early warning system," *Engineering Geology*, vol. 147–148, pp. 124–136, 2012, doi: 10.1016/j.enggeo.2012.07.017.

[9] C. Y. Hong, Y. F. Zhang. L. M. G. Leung, B. Forbes, N. Vlachopoulos, A. J. Hyett, F. C. Dai, and Y.Y. Ngai, "FBG-based monitoring of geohazards: Current status and trends," *Sensors and Actuators, A: Physical*, vol. 296, no. 1, pp. 132–144, 2017, doi: 10.3390/s17030452.

[10] Y. L. Wang, B. Shi, T. L. Zhang, H. H. Zhu, Q. Jie, and Q. Sun, "Introduction to an FBG-based inclinometer and its application to landslide monitoring," *Journal of Civil Structural Health Monitoring*, vol. 5, no. 5, pp. 645–653, 2015, doi: 10.1007/s13349-015-0129-4.

[11] H. Xu, F. Li, W. Zhao, S. Wang, Y. Du, and C. Bian, "A high precision fiber Bragg grating inclination sensor for slope monitoring," *Journal of Sensors*, vol. 2019, p. 7, 2019, doi: 10.1155/2019/1354029.

[12] D. Balageas, S. Bourasseau, M. Dupont, E. Bocherens, V. Dewynter-Marty, and P. Ferdinand, "Comparison between non-destructive evaluation techniques and integrated fiber optic health monitoring systems for composite sandwich structures," *Journal of Intelligent Material Systems and Structures*, vol. 11, no. 6, pp. 426–437, 2000, doi: 10.1106/MFM1-C5FT-6BM4-AFUD.

[13] G. Cumunel, S. Delepine-Lesoille, and P. Argoul, "Long-gauge optical fiber extensometers for dynamic evaluation of structures," *Sensors and Actuators, A: Physical*, vol. 184, pp. 1–15, 2012, doi: 10.1016/j.sna.2012.06.005.

[14] J. L. C. Diniz, R. D. Vieira, J. T. Castro, A. C. Benjamin, and J. L. F. Freire, "Stress and strain analysis of pipelines with localized metal loss," *Experimental Mechanics*, vol. 46, no. 6, pp. 765–775, 2006, doi: 10.1007/s11340-006-9826-6.

[15] C. Hong, Y. Zhang, Z. Lu, and Z. Yin, "A FBG tilt sensor fabricated using 3D printing technique for monitoring ground movement," *IEEE Sensors Journal*, vol. 19, no. 15, pp. 6392–6399, 2019, doi: 10.1109/JSEN.2019.2908873.

[16] L. Fang, T. Chen, R. Li, and S. Liu, "Application of embedded fiber Bragg grating (FBG) sensors in monitoring health to 3D printing structures," *IEEE Sensors Journal*, vol. 16, no. 17, pp. 6604–6610, 2016, doi: 10.1109/JSEN.2016.2584141.

[17] J. Frieden, J. Cugnoni, J. Botsis, T. Gmür, and D. Ćorić, "High-speed internal strain measurements in composite structures under dynamic load using embedded FBG sensors," *Composite Structures*, vol. 92, no. 8, pp. 1905–1912, 2010, doi: 10.1016/j.compstruct.2010.01.007.

[18] X. Gu, R. Hussain, H. Lu, and M. Zhou, "Fiber Bragg grating sensors for failure detection of flip chip ball grid array in four-point bend tests," *IEEE Sensors Journal*, vol. 9, no. 4, pp. 457–463, 2009, doi: 10.1109/JSEN.2009.2014419.

[19] Z. Lu, C. Hong, Y. Zhang, D. Su, and Y. Fu, "Development of an FBG sensor for measuring large range and multi-directional settlement," *IEEE Photonics Journal*, vol. 7, no. 8, pp. 669–677, 2019, doi: 10.1109/ACCESS.2019.2932774.

[20] M. Maheshwari, Y. Yang, D. Upadrashta, E. S. Huang, and K. H. Goh, "Fiber Bragg grating (FBG) based magnetic extensometer for ground settlement monitoring," *Sensors and Actuators*, vol. 296, pp. 132–144, 2019, doi: 10.1016/j.sna.2019.06.053.

[21] J. Q. Qin, W. Q. Feng, P. C. Wu, and J. H. Yin, "Fabrication and performance evaluation of a novel FBG-based effective stress cell for directly measuring effective stress in saturated soils," *Measurement: Journal of the International Measurement Confederation*, vol. 155, no. 2, pp. 1–9, 2020, doi: 10.1016/j.measurement.2020.107491.

[22] Q. Wang, J. Huang, Q. Liu, and Z. Zhou, "Dynamic strain measurement of hydraulic system pipeline using fibre Bragg grating sensors," *Advances in Mechanical Engineering*, vol. 8, no. 4, pp. 1–8, 2016, doi: 10.1177/1687814016645069.

[23] C. E. Campanella, A. Cuccovillo, C. Campanella, A. Yurt, and V. M. N. Passaro, "Fibre Bragg grating based strain sensors: Review of technology and applications," *Journal of Sensors*, vol. 18, no. 9, 2018, doi: 10.3390/s18093115.

[24] M. C. Emmons, S. Karnani, S. Trono, K. P. Mohanchandra, W. L. Richards, and G. P. Carman, "Strain measurement validation of embedded fiber Bragg gratings," *International Journal of Optomechatronics*, vol. 4, no. 1, pp. 22–33, 2010, doi: 10.1080/15599611003649984.

[25] S. W. Park, D. H. Kang, H. J. Bang, S. O. Park, and C. G. Kim, "Strain monitoring and damage detection of a filament wound composite pressure tank using embedded fiber Bragg grating sensors," *Key Engineering Materials*, vol. 321–323, no. 10, pp. 182–185, 2006, doi: 10.4028/www.scientific.net/kem.321-323.182.

[26] H. Gnewuch, E. Smeu, D. A. Jackson, and A. G. Podoleanu, "Long range extensometer for civil structure monitoring using fibre Bragg gratings," *Measurement Science and Technology*, vol. 16, no. 10, pp. 2005–2010, 2005, doi: 10.1088/0957-0233/16/10/016.

[27] A. Huang, C. C. Wang, J. T. Lee, and Y. Ho, "Applications of FBG-based sensors to ground stability monitoring," *Journal of Rock Mechanics and Geotechnical Engineering*, vol. 8, no. 4, pp. 513–520, 2016, doi: 10.1016/j.jrmge.2016.01.007.

[28] M. H. Yau, T. H. T. Chan, D. P. Thambiratnam and H. Y. Tam, "Using fiber Bragg grating (FBG) sensors for vertical displacement measurement of bridges," *Journal of Optoelectronics and Advanced Materials*, vol. 16, no. 4, pp. 1604–1609, 2006.

[29] P. Ferdinand, S. Magne, V. Dewynter-Marty, C. Martinez, S. Rougeault, and M. Bugaud, "Applications of Bragg grating sensors in Europe," *Journal of the Optical Society of America B*, vol. 16, no. 1, pp. 14–19, 1997.

[30] Y. Zhang and L. Borana, "Design, fabrication and testing of a 3D printed FBG pressure sensor," *IEEE Access*, vol. 7, no. 10, pp. 38577–38583, 2019, doi: 10.1109/ACCESS.2019.2905349.

[31] A. G. Leal-Junior, C. Marques, M. R. N. Ribeiro, M. J. Pontes, and A. Frizera, "FBG-embedded 3-D printed ABS sensing pads: The impact of infill density on sensitivity and dynamic range in force sensors," *IEEE Sensors Journal*, vol. 18, no. 20, pp. 8381–8388, 2018, doi: 10.1109/JSEN.2018.2866689.

[32] G. Pereira, C. Frias, H. Faria, O. Frazão, and A. T. Marques, "On the improvement of strain measurements with FBG sensors embedded in unidirectional composites," *Polymer Testing*, vol. 32, no. 1, pp. 99–105, 2013, doi: 10.1016/j.polymertesting.2012.09.010.

[33] H. Tian, D. guang Liu, Y. ping Wang, and Q. lin Wang, "Effect of adhesive type on the sensitivity coefficient of FBG sensor bonded on the surface of CFRP," *Optoelectronics Letters*, vol. 15, no. 4, pp. 264–268, 2019, doi: 10.1007/s11801-019-8183-5.

[34] M. M. Carroll, "PVC (polyvinylchloride) pipe reliability and failure modes.," *Journal of Composite Materials*, vol. 13, no. 4, pp. 11–21, 1984.

[35] P. Shirish, T. Kelkar, and B. S. A, "Mulching: A soil and water conservation practice," *Research Journal of Agriculture and Forestry Sciences*, vol. 1, no. 3, pp. 26–29, 2013

[36] M. K. Neelam and S. Kalaga, "Elastic properties of PVC pipes," *Journal of Structural Engineering (Madras)*, vol. 29, no. 2, pp. 91–96, 200

M. A. Alias received the Bachelor of Science (Hons) in Industrial Physics from the Faculty of Science, Universiti Teknologi Malaysia (UTM), Johor, Malaysia in 2020. He is currently a postgraduate student and a research assistant at Photonics Research Centre, University of Malaya, Kuala Lumpur, Malaysia. His current research interest focuses on optical fiber sensors mainly on fiber Bragg grating

M. F. Ismail obtained his Bachelor of Engineering (Telecommunication) from the Faculty of Engineering, University of Malaya, Kuala Lumpur, Malaysia in 1999 and Master of Engineering (Science) from the Faculty of Engineering, University of Malaya in 2004. He obtained his Ph.D. from the same university in 2021 where his research focuses on pulsed, multiwavelength fibre lasers and waveguide.

M. S. M. Sa'ad received the Bachelor of Science (Hons) in Pure Physics from the Faculty of Science, University of Malaya, Kuala Lumpur, Malaysia in 2019. He is currently a postgraduate student and a research assistant at the Photonics Research Centre, University of Malaya, Kuala Lumpur, Malaysia. His research interest focuses on fiber optic sensors mainly on fiber Bragg gratings.

M. K. A. Zaini received the bachelor's degree from the Department of Physics, Faculty of Science, University Putra Malaysia, Selangor, Malaysia, in 2015, and currently a postgraduate candidate at Photonics Research Centre, University of Malaya, Kuala Lumpur, Malaysia. His current research interest includes fiber Bragg grating sensors, and Spatial Division Multiplexing.

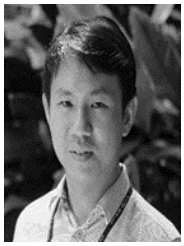

K. S. Lim received his Bachelor of Engineering degree from the Department of Electrical Engineering, Faculty of Engineering, University of Malaya, Kuala Lumpur. Malaysia, in 2008, and the Ph.D. degree from the Photonics Research Centre, Department of Physics, University of Malaya, in 2012. He is currently a Senior Lecturer with Photonics Research Centre, University of Malaya. His current research interests include fiber Bragg grating sensors, spatial division multiplexing, and laser medical devices. He is a Corporate Member of the Institute of Engineers Malaysia (IEM), a registered Professional Engineer (Telecommunication) of the Board of Engineers Malaysia (BEM), and a member of OSA.

K. T. V. Grattan graduated in Physics from Queen's University Belfast with a BSc (First Class Honours) in 1974, followed by a Ph.D. in Laser Physics. His doctoral research involved the use of laser-probe techniques for measurements on potential new laser systems. He obtained the degree of Doctor of Science (DSc) from City University in 1992 for his sensor work. His research interests have expanded to include the development and use of fiber optic and optical systems in the measurement of a range of physical and chemical parameters.

G. Brambilla is a professor at the Optoelectronics Research Centre and, since 2016, co-Director and General Manager of the Future Photonics Hub. He has been Director of the Centre for Innovative Manufacturing in Photonics until 2015. He obtained his MSc (Engineering) with honors from Politecnico di Milano (Italy) in 1996 and his PhD degree in Optoelectronics from the University of Southampton in 2002. In 2007 he was awarded the Royal Society Research Fellowship, which was then extended in 2012. His research interests include optical fiber sensors; optical fiber structuring using fs lasers; specialty and polymer fibers; new fiber fabrication technologies; UV fiber lasers; devices based on optical fiber nanowires, fiber tapers and couplers; rare earth doped scintillating fibers and fibers for nuclear sensing.

B. M. A. Rahman received BSc Eng. and MSc Eng. degrees in Electrical Engineering with distinctions from Bangladesh University of Engineering and Technology (BUET), Dhaka, Bangladesh, in 1976 and 1979, respectively He received his PhD degree in Electronic Engineering from University College, London in 1982. From 1976 to 1979, he was a Lecturer at the Electrical Engineering Department, BUET. In 1988, he joined the Electrical, Electronic and Information Engineering Department of City University, London, as a Lecturer, where he is now a professor. At City University, London, he leads the research group on Photonics Modelling, specialized in the development and use of the rigorous and full-vectorial numerical approaches, frequency domain modal solution approach, the beam propagation method, and time-domain approach, primarily based on the numerically efficient finite element method.

S. A. Reduan received the Bachelor of Science (Hons) in Physics from the Faculty of Science, Universiti Teknologi Malaysia (UTM), Johor, Malaysia in 2015. She received her Ph.D. from Universiti Malaya in 2020 where her research focuses on pulsed laser, saturable absorber and fluoride fiber-based laser.

H. Ahmad received the Ph.D. degree in laser technology from the University of Wales, Swansea, U.K., in 1983. He is currently a Professor with the Department of Physics and director of the Photonics Research Centre, University of Malaya, Kuala Lumpur, Malaysia, where he has actively pursued research activities in the field of photonics since 1983. He is the author of more than 400 professional papers in international journals and conference proceedings. His research interests are in lasers, fiber-based devices for telecommunications, and fiber-based sensor devices. Dr. Ahmad is a Fellow of the Academy of Sciences, Malaysia.